Registration of Lung Surface Proximity for Assessment of Pleural Thickenings

Peter Faltin[1], Kraisorn Chaisaowong[1,2], Thomas Kraus[3], Til Aach[1]

[1]Lehrstuhl für Bildverarbeitung, RWTH Aachen University
[2]King Mongkut's University of Technology North Bangkok
[3]Institut für Arbeitsmedizin und Sozialmedizin, UK Aachen
peter.faltin@lfb.rwth-aachen.de

Abstract. Follow-up assessment of pleural thickenings requires the comparison of information from different points in time. The investigated image regions must be precisely registered to acquire this information. Since the thickenings' growth is the target value, this growth should not be compensated by the registration process. We therefore present a non-rigid registration method, which preserves the shape of the thickenings. The deformation of the volume image is carried out using B-splines. With focus on the image regions located around the lung surface, an efficient way of calculating corresponding points combined with the reuse of information from different scale levels leads to the non-rigid registration, which can be performed within a short computation time.

1 Introduction

Inhaled carcinogenic asbestos fibers can cause pleural thickenings which may evolve to pleural mesothelioma. To reduce the mortality, an early stage diagnosis is essential. Hence high-risk patients undergo a regular medical check-up including CT imaging. Manual analysis of CT data is time consuming and subject to strong inter- and intra-reader variability [1]. The application of a computer assisted diagnosis system reduces the workload and provides objective analysis. Within this framework a non-rigid registration is required to compare information from multiple points in time. The system is designed for the clinical routine. Therefore all algorithms are designed with respect to their computation time.

B-spline registration utilizes different methods to determine the mesh, controlling the deformation. Rueckert et al. [2] use mutual information while Loeckx et al. [3] use conditional mutual information to iteratively optimize the mesh. Faster methods like Chui et al. [4] or Kwon et al. [5] utilize features to calculate the deformation, but are still based on iterative optimization schemes. These methods however are not capable to protect the thickening growth from being undesirably compensated. We explicitly address this problem and additionally calculate the transformed mesh from matched points non-iteratively.

2 Materials and Methods

The images $\boldsymbol{G}_t^{(0)}, t \in \{0,1\}$ from the same patient at two different points in time consist of the voxels $\boldsymbol{G}_t^{(0)}(\boldsymbol{r})$, with the image coordinates $\boldsymbol{R}^{(0)} = \{(x,y,z)^T : 0 \leq x < X^{(0)}, 0 \leq y < Y^{(0)}, 0 \leq z < Z^{(0)}\}$. The superscripts $^{(0)}$ address the scaling level and can be ignored for the first step. The lung masks $\boldsymbol{R}_{\mathrm{L},t}^{(0)} \subset \boldsymbol{R}^{(0)}$ and the associated surfaces $\boldsymbol{\partial R}_{\mathrm{L,t}}^{(0)}$ are extracted using two-step supervised range-constrained Otsu thresholding [6]. The thickenings $\boldsymbol{R}_{\mathrm{T},t=0}^{(0)} \subset \boldsymbol{R}^{(0)}$ for $t = 0$ are segmented by the comparison of the actual lung with a healthy lung model [6]. With the known mask data $\boldsymbol{R}_{\mathrm{L},t}^{(0)}$, the rigid transformation $\boldsymbol{T}_{\mathrm{r}}$ can be determined using e.g. a Gibbs-Markov random field based approach from Faltin et al. [7].

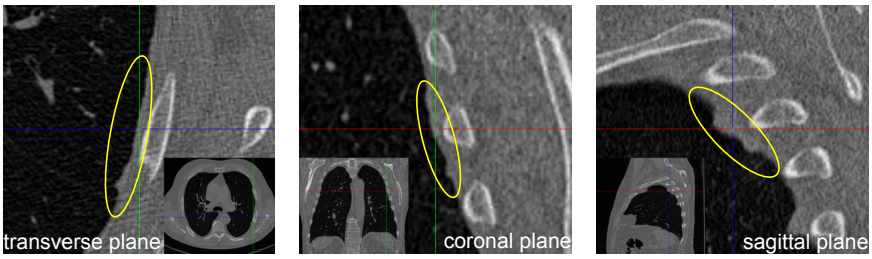

Fig. 1. A pleural thickening shown in different planes.

We present here an efficient method for the non-rigid part of the registration. First, the surface of interests (SOI) is extracted. The local registration for each included point is identified and the image is deformed accordingly. Offsets and deformations are determined for each scaling level of an image pyramid.

2.1 Extracting the Surface of Interest

As shown in fig. 1, it is hard to distinguish between the healthy lung boundary and the boundary implied by a pleural thickening. Therefore the thickening growth can easily been misinterpreted as a deformation. The critical thickening regions $\boldsymbol{R}_{\mathrm{T},t}^{(0)} \subset \boldsymbol{R}^{(0)}$ are first increased by a dilation with a sphere $\boldsymbol{W}$ of radius 5 (voxels) and then masked in the point-set approximating the lung surface $\boldsymbol{\partial R}_{\mathrm{L,t}}^{(0)}$. This leads to the discrete SOI

$$\boldsymbol{R}_{\mathrm{SOI},t}^{(0)} = \boldsymbol{\partial R}_{\mathrm{L},t}^{(0)} \setminus (\boldsymbol{R}_{\mathrm{T},t}^{(0)} \oplus \boldsymbol{W}), \tag{1}$$

which contains the voxel coordinates at lung surface excluding regions close to thickenings.

2.2 Applying the Image Pyramid

The unregistered and downsampled images of the lungs are determined iteratively applying $\boldsymbol{G}_t^{(q)} = \mathrm{B}_{\downarrow 2}\{\boldsymbol{G}_t^{(q-1)}\}$, where q, $0 < q < Q$, denotes the scaling level and $\boldsymbol{R}^{(q)}$ its image domain for each of the Q scaling levels. $\mathrm{B}_{\downarrow 2}$ includes downsampling of factor 2 and a previous smoothing with an appropriate Gaussian kernel. Analogue to the Gaussian kernel which prevents aliasing in the image, a rounding operation is applied, when downsampling the point-set of the SOI, to keep all surface information

$$\boldsymbol{R}_{\mathrm{SOI},t}^{(q)} = \left\{ \left\lfloor \frac{\boldsymbol{r}^{(q-1)}}{2} \right\rfloor : \boldsymbol{r}^{(q-1)} \in \boldsymbol{R}_{\mathrm{SOI},t}^{(q-1)} \right\}, 0 < q < Q. \tag{2}$$

2.3 Determining the Local Displacements

The data obtained from the image pyramid at level q is modified considering the results from the previous level $(q+1)$, which is denoted by a tilde on top of the identifiers and described in section 2.4. The deformation is determined at each level q in the SOI by 3D block matching. As an error metric the sum of absolute differences is calculated

$$\mathbf{SAD}^{(q)}(\boldsymbol{d}, \boldsymbol{r}) = \sum_{\|\boldsymbol{r}'-\boldsymbol{r}\|_\infty \leq b, \boldsymbol{r}' \in \mathbb{Z}^3} \left| \tilde{\boldsymbol{G}}_{t=0}^{(q)}(\boldsymbol{r}' + \boldsymbol{d}) - \boldsymbol{G}_{t=1}^{(q)}(\boldsymbol{r}') \right|, \boldsymbol{r} \in \tilde{\boldsymbol{R}}_{\mathrm{SOI},t=0}^{(q)}, \tag{3}$$

for each displacement $\boldsymbol{d}$, with the block size b. For densely sampled surfaces and large block dimensions $(2b+1)^3$, overlapping of the blocks results in multiple calculation of the absolute differences. An more efficient way is to separately create an error image and summing up the differences. An error image

$$\boldsymbol{E}^{(q)}(\boldsymbol{d}, \boldsymbol{r}) = \left| \tilde{\boldsymbol{G}}_{t=0}^{(q)}(\boldsymbol{r} + \boldsymbol{d}) - \boldsymbol{G}_{t=1}^{(q)}(\boldsymbol{r}) \right|, \boldsymbol{r} \in \boldsymbol{R}^{(\boldsymbol{q})}, \tag{4}$$

is created for each displacement $\boldsymbol{d} \in \{\boldsymbol{s}; \forall \boldsymbol{s} \in \mathbb{Z}^3, \|(0,0,0)^T - \boldsymbol{s}\|_\infty \leq 1\}$, which includes all 27 combinations of displacements $\{-1, 0, 1\}$ per dimension. Calculating the error for the full image domain $\boldsymbol{R}^{(\boldsymbol{q})}$ in parallel can be faster than to determine which voxels are required for the block-wise calculation and individually addressing them. Larger displacements are implicitly considered due to the image pyramid. The computationally intensive summation is only applied for the SOI, resulting in the SAD for each displacement $\boldsymbol{d}$,

$$\mathbf{SAD}^{(q)}(\boldsymbol{d}, \boldsymbol{r}) = \sum_{\|\boldsymbol{r}'-\boldsymbol{r}\|_\infty \leq b, \boldsymbol{r}' \in \mathbb{Z}^3} \boldsymbol{E}^{(q)}(\boldsymbol{d}, \boldsymbol{r}'), \boldsymbol{r} \in \tilde{\boldsymbol{R}}_{\mathrm{SOI},t=0}^{(q)}. \tag{5}$$

Finally for each feature point the displacement $\boldsymbol{D}$ is determined choosing the displacement, which minimizes the SAD

$$\boldsymbol{D}^{(q)}(\boldsymbol{r}) = \arg\min_{\boldsymbol{d}} \mathbf{SAD}^{(q)}(\boldsymbol{d}, \boldsymbol{r}), \boldsymbol{r} \in \tilde{\boldsymbol{R}}_{\mathrm{SOI},t=0}^{(q)}. \tag{6}$$

2.4 Deforming the Images

The deformed image $\boldsymbol{G}_{t=0}^{(q)}$ can be interpolated using B-splines, which are controlled by a mesh of $N_x \times N_y \times N_z$ points $\tilde{\boldsymbol{\Phi}}_{\mu,\nu,\epsilon}^{(q)}$, with the uniform spacing δ. The positions of these control points are determined by the B-spline approximation (BA) of Lee et al. [8], which utilizes the SOI $\boldsymbol{R}_{\mathrm{SOI},t=0}^{(q)}$ and the associated displacements $\boldsymbol{D}^{(q)}(\boldsymbol{r})$. The deformation for each image point is given by

$$\boldsymbol{T}_{\mathrm{nr}}^{(q)}(\boldsymbol{r}) = \begin{cases} \sum_{l=0}^{3}\sum_{m=0}^{3}\sum_{n=0}^{3} B_l(u)B_m(v)B_n(w)\tilde{\boldsymbol{\Phi}}_{i+l,j+m,k+n}^{(q)} & 0 < q < Q-1 \\ \boldsymbol{r} & q = Q-1 \end{cases}, \quad (7)$$

with $i = \lfloor \frac{x}{N_x} \rfloor + 1$, $j = \lfloor \frac{y}{N_y} \rfloor + 1$, $k = \lfloor \frac{z}{N_z} \rfloor + 1$, $u = \frac{x}{N_x} - \lfloor \frac{x}{N_x} \rfloor$, $v = \frac{y}{N_y} - \lfloor \frac{y}{N_y} \rfloor$, $w = \frac{z}{N_z} - \lfloor \frac{z}{N_z} \rfloor$. $B_c(s)$ is the c-th basis function of the cubic and uniform B-spline [2]. To avoid iterative interpolations for the following scale levels we adapt the control points using

$$\tilde{\boldsymbol{\Phi}}_{\mu,\nu,\epsilon}^{(q)} = 2 \cdot \boldsymbol{T}_{\mathrm{nr}}^{(q+1)}\left(\frac{\boldsymbol{\Phi}_{\mu,\nu,\epsilon}^{(q)}}{2}\right). \quad (8)$$

Therefore the transformed image data and SOI from the first point in time ($t = 0$) are given by

$$\tilde{\boldsymbol{G}}_{t=0}^{(q)}(\boldsymbol{r}) = \boldsymbol{G}_{t=0}^{(q)}\left(2 \cdot \boldsymbol{T}_{\mathrm{nr}}^{(q+1)}\left(\frac{\boldsymbol{r}}{2}\right)\right), \boldsymbol{r} \in \boldsymbol{R}^{(q)} \quad (9)$$

and

$$\tilde{\boldsymbol{R}}_{\mathrm{SOI},t=0}^{(q)} = \left\{ \left\lfloor 2 \cdot \boldsymbol{T}_{\mathrm{nr}}^{(q+1)}\left(\frac{\boldsymbol{r}}{2}\right) + (0.5, 0.5, 0.5)^T \right\rfloor : \boldsymbol{r} \in \boldsymbol{R}_{\mathrm{SOI},t=0}^{(q)} \right\}. \quad (10)$$

3 Results

The presented method is applied to CT datasets from 4 different patients. For each patient 2 CT scans from different points in time are non-rigidly registered. The CT scans for the patients I - III consist of 400-700 slices, while the the CT scans from patient IV consist of approx. 60 slices. The SAD within a lung surface proximity $\boldsymbol{R}_{P,t=1}$ is used as an indicator to evaluate the registration quality. After dilation with a sphere $\boldsymbol{W}$ of radius 10 (voxels) on the lungs surface $\boldsymbol{\partial R}_{t=1}$ the proximity $\boldsymbol{R}_{P,t=1} = \boldsymbol{\partial R}_{t=1} \oplus \boldsymbol{W}$ is created. Additionally the average surface distance (ASD), from each point of the lung surface $\tilde{\boldsymbol{R}}_{\mathrm{SOI},t=0}^{(0)}$ to the closest point in $\boldsymbol{R}_{\mathrm{SOI},t=1}^{(0)}$ is determined.

First we investigate the results using varying block size b (fixed $\delta = 8$) then mesh spacing δ (fixed $b = 4$). The resulting SAD are shown in fig. 2.

Finally we compare the performance of our method to the implementation from Kroon (MATLAB central file ID: #20057). SAD and ASD are compared in fig. 3 for both methods and all patients. We chose for patient I - III $\delta = 8$, $b = 8$ and for patient IV with the low slice count $\delta = 4$, $b = 4$.

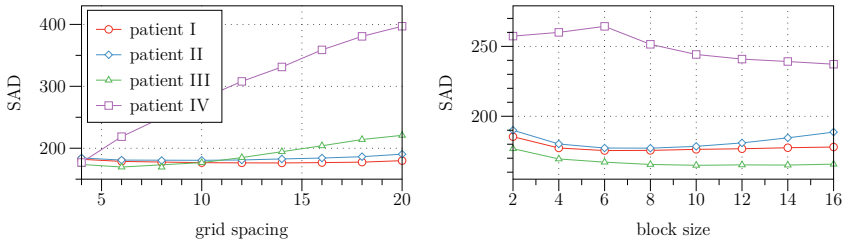

Fig. 2. SAD using different parameters.

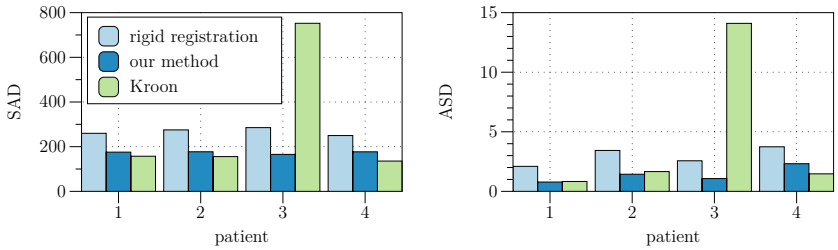

Fig. 3. Comparison of the Kroon implementation and our approach.

4 Discussion

Fig. 2 shows that our method does not optimally perform for patient IV, which is a consequence of the low slice count. For higher slice count the method shows a stable and low SAD for the parameter $\delta = 8$, $b = 8$. Visual examples of the results are shown as difference images in fig. 5. The rigid registration 5(a) performs an overall optimization and is not optimal for each individual part of the lung surface. The visualizations of the non-rigid results both 5(b) show 5(c) good performance in the surface regions. While our approach 5(b) shows weaknesses in the disregarded image regions, the Kroon approach 5(c) performs well for whole image.

Comparing our approach to the Kroon implementation in fig. 3 reveals that the SAD values are in a similar range. As expected our implementation performs

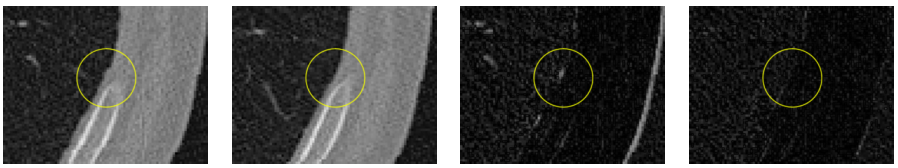

(a) our aproach (b) Kroon (c) our approach (d) Kroon

Fig. 4. Visible thickening growth influenced by non-rigid registration comparing CT image data (a),(b) and difference images (c),(d).

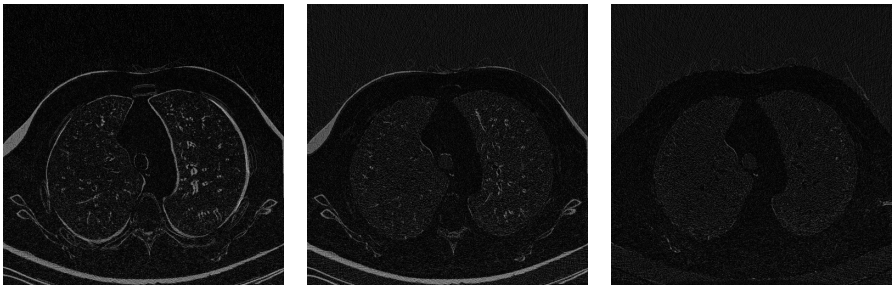

(a) rigid registration (b) our aproach (c) Kroon

Fig. 5. Visual comparison of registrations by regarding the difference image.

for SAD slightly worse, because it intentionally does not compensate thickening deformations, as shown in figure 4. For ASD our algorithm performs slightly better except for patient IV. The method of Kroon fails for patient III.

For clinical routine, computation time is an important aspect. Both Kroon's and our algorithm are realized as MATLAB and C hybrid implementations and tested on a standard Desktop Computer (2.67 GHz Core i5, 8GB memory). The iterative Kroon implementation takes several days for the registration process, while our approach takes at maximum 2.5 minutes.

For future work we plan to use the obtained registration for a consistent segmentation of the thickenings at both points in time.

References

1. Ochsmann E, Carl T, Brand P, Raithel H, Kraus T. Inter-reader variability in chest radiography and HRCT for the early detection of asbestos-related lung and pleural abnormalities in a cohort of 636 asbestos-exposed subjects. Int Arch Occup Environ Health. 2010;83:39–46.
2. Rueckert D, Sonoda LI, Hayes C, Hill DLG, Leach MO, Hawkes DJ. Nonrigid registration using free-form deformations: Application to breast MR images. IEEE Trans Med Imaging. 1999;18:712–721.
3. Loeckx D, Slagmolen P, Maes F, Vandermeulen D, Suetens P. Nonrigid image registration using conditional mutual information. IEEE Trans Med Imaging. 2007;29(1):725–737.
4. Chui H, Win L, Schultz R, Duncan JS, Rangarajan A. A unified non-rigid feature registration method for brain mapping. Medical Image Analysis. 2003;7(2):113–30.
5. Kwon D, Yun ID, Lee KH, Lee SU. Efficient Feature-Based Nonrigid Registration of Multiphase Liver CT Volumes. In: BMVC; 2008. .
6. Chaisaowong K, Bross B, Knepper A, Kraus T, Aach T. Detection and Follow-Up Assessment of Pleural Thickenings from 3D CT Data. In: ECTI; 2008. p. 489–492.
7. Faltin P, Chaisaowong K, Kraus T, Aach T. Markov-Gibbs Model Based Registration of CT Lung Images Using Subsampling for the Follow-Up Assessment of Pleural Thickenings. In: IEEE ICIP; 2011. p. 2229–2232.
8. Lee S, Wolberg G, Shin SY. Scattered Data Interpolation with Multilevel B-Splines. IEEE Trans Vis Comput Graph. 1997;3:228–244.